

# Applying NOX Error Mitigation Protocols to Calculate Real-time Quantum Field Theory Scattering Phase Shifts

Zachary Parks<sup>1</sup>, Arnaud Carignan-Dugas<sup>2</sup>, Patrick Dreher<sup>3 4 \*</sup>, Erik Gustafson<sup>5</sup>, and Yannick Meurice<sup>6</sup>

<sup>1</sup> Department of Computer Science, North Carolina State University, Raleigh, NC 27695, USA

<sup>2</sup> Keysight Technologies Canada, Kanata, ON K2K 2W5, Canada

<sup>3</sup> Department of Electrical and Computer Engineering,

North Carolina State University, Raleigh, NC 27695, USA

<sup>4</sup> Department of Physics, North Carolina State University, Raleigh, NC 27695, USA

<sup>5</sup> Fermi National Accelerator Laboratory, Batavia, Illinois 60510, USA

<sup>6</sup> Department of Physics and Astronomy, The University of Iowa, Iowa City, IA 52242, USA and

\*Corresponding Author: email: padreher@ncsu.edu

Real-time scattering calculations on a Noisy Intermediate Scale Quantum (NISQ) quantum computer are disrupted by errors that accumulate throughout the circuits. To improve the accuracy of such physics simulations, one can supplement the application circuits with a recent error mitigation strategy known as Noisy Output eXtrapolation (NOX). We tested these error mitigation protocols on a Transverse Field Ising model and improved upon previous calculations of the phase shift. Our proof-of-concept 4-qubit application circuits were run on several IBM quantum computing hardware architectures. Metrics were introduced that show between 21% and 74% error reduction for circuit depths ranging from 14 to 37 hard cycles, confirming that the NOX technique applies to circuits with a broad range of failure rates. This observation on different cloud-accessible devices further confirms that NOX provides performance improvements even in the advent where circuits are executed in substantially time-separated batches. Finally, we provide a heuristic method to obtain systematic error bars on the mitigated results, compare them with empirical errors and discuss their effects on phase shift estimates.

Recent advances in quantum computing have piqued the interest of physicists working in high energy, nuclear and condensed matter physics. It is expected that in the coming years, quantum computers will be used to attack physics problems that are not amenable to solution using classical computers. Examples of such problems include modelling of high energy particle physics real-time scattering experiments, dynamical processes in nuclear astrophysics describing neutron star evolution and emergent low-energy phenomena in condensed matter systems [1–7].

There have been several recent projects focused on real time evolution of the quantum Ising model (QIM) on a limited number of sites [8–22], as well as more complicated high energy and nuclear physics Hamiltonians [6, 23–82]. For the QIM, phase shifts have been calculated from the time delay of a wave packet due to interactions, using the real-time evolution in the early and intermediate stages of the collision [83]. These calculations were performed with four qubits on IBMQ and trapped ion platforms. Simple error suppression methods [11] as well as using significantly larger Trotter steps [10, 84, 85] than suggested by rigorous bounds, provided reasonable extrapolation for scattering times up to the order of the approximate periodicity of the problem.

In this work, three compounding error suppression techniques were implemented: readout calibration (RCAL) [86–93], randomized compiling (RC)

[94], and Noiseless Output eXtrapolation (NOX) [95]. The circuits' generation and the analysis related to those three mitigation techniques were performed by the True-Q software [96]. RCAL is implemented using a few quantum circuits to estimate the noise matrix associated with the measurement step [86–93]. The inverse noise matrix is then applied to subsequent outcome distributions, which effectively suppresses measurement errors. RC and NOX are targeted toward suppressing the effect of errors occurring during *computation cycles*. A computation cycle, hereafter referred to as a cycle, is defined broadly as a set of instructions performed on a processing unit over a time interval (for instance, a round of parallel CNOT gates). For a more detailed introduction to cycles, see appendix B.

Recall that quantum computers output an outcome following a probability distribution. The overarching idea behind error suppression (to contrast with error correction) is to pair noisy application circuits with other circuits and combine the probabilistic results in such a way that the desired observable estimate is closer to the ideal expectation value.

The role of RC is to regulate the propagation of cycle errors throughout the computation. Often, the regulation effect substantially reduces the overall circuit failure rate over ungoverned circuits [97–99]. The principle behind RC is to replace an application circuit that is meant to be run  $N_{\text{shots}}$  times

with  $n_{\text{rand}}$  equivalent circuits sampled over a particular random distribution, each to be performed  $N_{\text{shots}}/n_{\text{rand}}$  times (in our case we chose  $n_{\text{rand}} = 30$  circuit randomizations). A well-known effect of RC is that it effectively tailors general Markovian error sources into stochastic error channels. That is if we divide a circuit into appropriate cycles [100],  $\mathcal{C}_{\text{ideal}} = C_m \cdots C_2 C_1$ , the average RC circuit can be well approximated as a sequence of ideal cycles interleaved with Pauli stochastic error channels  $\mathcal{E}_i$ ,

$$\langle \mathcal{C} \rangle_{\text{RC}} \simeq \mathcal{E}_m C_m \cdots \mathcal{E}_2 C_2 \mathcal{E}_1 C_1, \quad (1)$$

where the action of  $\mathcal{E}_i$  on a state  $\rho$  is defined as

$$\mathcal{E}_i[\rho] = \sum_j p_j(C_i) P_j \rho P_j^\dagger, \quad (2)$$

where  $P_j$  are Pauli operators and  $\{p_j(C_i)\}_j$  is an error probability distribution. The error profile  $\{p_j(C_i)\}_j$  is proper to the noisy device under consideration and generally depends on the cycle  $C_i$ , since some operations are more error-prone than others.

On top of RC, we performed an error mitigation scheme introduced in [95] known as NOX. In practice, the intended scattering circuit is run jointly with a family of noise-amplified versions thereof, each of which is randomized via RC:

$$\begin{aligned} \langle \mathcal{C} \rangle_{\text{RC}} &\simeq \mathcal{E}_m C_m \cdots \mathcal{E}_2 C_2 \mathcal{E}_1 C_1, \\ &\quad (\text{Non-amplified RC circuit}) \\ \langle \mathcal{C}_1 \rangle_{\text{RC}} &\simeq \mathcal{E}_m C_m \cdots \mathcal{E}_2 C_2 \mathcal{E}_1^{1+\alpha} C_1, \\ &\quad (\mathcal{E}_1\text{-amplified circuit}) \\ \langle \mathcal{C}_2 \rangle_{\text{RC}} &\simeq \mathcal{E}_m C_m \cdots \mathcal{E}_2^{1+\alpha} C_2 \mathcal{E}_1 C_1, \\ &\quad (\mathcal{E}_2\text{-amplified circuit}) \\ &\vdots \\ \langle \mathcal{C}_m \rangle_{\text{RC}} &\simeq \mathcal{E}_m^{1+\alpha} C_m \cdots \mathcal{E}_2 C_2 \mathcal{E}_1 C_1. \\ &\quad (\mathcal{E}_m\text{-amplified circuit}) \end{aligned}$$

As indicated via the  $\langle \cdot \rangle_{\text{RC}}$  notation, each of the  $m+1$  above circuits is averaged via RC to ensure that the effective error model remains Pauli stochastic. In our case, the error amplification  $\mathcal{E}_i \rightarrow \mathcal{E}_i^{1+\alpha}$  is approximately obtained by replacing a cycle of parallel CX gates with a circuit-equivalent odd sequence of identical CX cycles, interleaved with randomly compiled Pauli operations. We chose a repetition number of 11 CX cycles, corresponding to an amplification parameter of  $\alpha = 10$ .

Given an observable  $O$ , we denote its expected value given an effective RC circuit  $\langle \mathcal{C} \rangle_{\text{RC}}$  as  $\mathbb{E}(O | \langle \mathcal{C} \rangle_{\text{RC}})$ . With this notation at hand, the RC

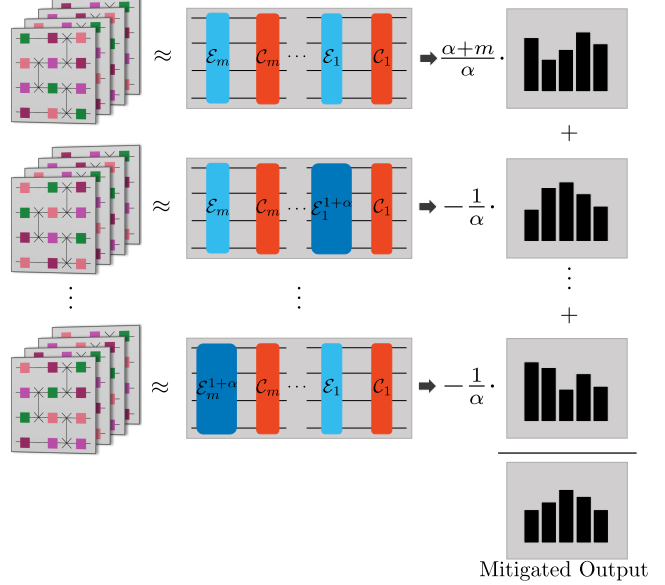


Figure 1: Overview of the RC+NOX procedure. The application circuit is run jointly with a family of noise-amplified versions of itself, each of which is averaged via RC (left). Each set of RC circuits can be approximated (middle) as a sequence of ideal cycles  $\mathcal{C}_i$  (red) interleaved with non-amplified  $\mathcal{E}_i$  (cyan) and amplified Pauli stochastic error channels  $\mathcal{E}_i^{1+\alpha}$  (dark blue). The individual distributions of the original and of each error-amplified RC circuit (right) are used to calculate a mitigated expectation value of a given observable  $O$  according to Eq. (4).

and RC+NOX estimates for  $O$  are, respectively:

$$\hat{O}_{\text{RC}} := \mathbb{E}(O | \langle \mathcal{C} \rangle_{\text{RC}}), \quad (3)$$

$$\begin{aligned} \hat{O}_{\text{RC+NOX}} &:= \frac{\alpha+m}{\alpha} \mathbb{E}(O | \langle \mathcal{C} \rangle_{\text{RC}}) \\ &\quad - \frac{1}{\alpha} \sum_{i=1}^m \mathbb{E}(O | \langle \mathcal{C}_i \rangle_{\text{RC}}). \end{aligned} \quad (4)$$

This RC+NOX procedure is pictorially illustrated in Fig. 1. Even in the limit of infinite sampling, NOX is not expected to return mitigated results that perfectly match the ideal distribution. Indeed, this mitigation technique performs a first-order correction. A more complete mathematical explanation is provided in [95] (see theorem 2), but we also included a brief analysis in appendix C.

As we now proceed to explain, this method yields significant error reduction for scattering probabilities  $P_{\pm}(t)$  to be in the  $|\pm k\rangle$  state for the QIM [83]. As reviewed in the SM and used hereafter, the nor-

malized reflection probability

$$R_-(t) \equiv \frac{P_-(t)}{P_+(t) + P_-(t)} \quad (5)$$

allows us to estimate time delays and phase shifts due to interactions.

Our dynamics simulations were performed on the IBM quantum hardware platform `ibmq_kolkata`. We targeted qubits 20, 19, 22, 25 on the 27-qubit `ibmq_kolkata` platform. The depths of the various circuits ranged from 14 to 37 native entangling cycles, thereby covering a wide scope of circuit failure rates. Moreover, the total number of circuits was high enough that our experiments had to be batched in multiple jobs, and effectively ran on the cloud over the course of many hours. The results from these calculations for  $R_-(t)$  obtained with NOX and previously used methods (called “bare” below) can be compared with the ideal values obtained by performing the three steps of the quantum computations with accurate numerical methods.

The differences with the ideal results are shown in Fig. 2 for the free `ibmq_kolkata` results. The signs

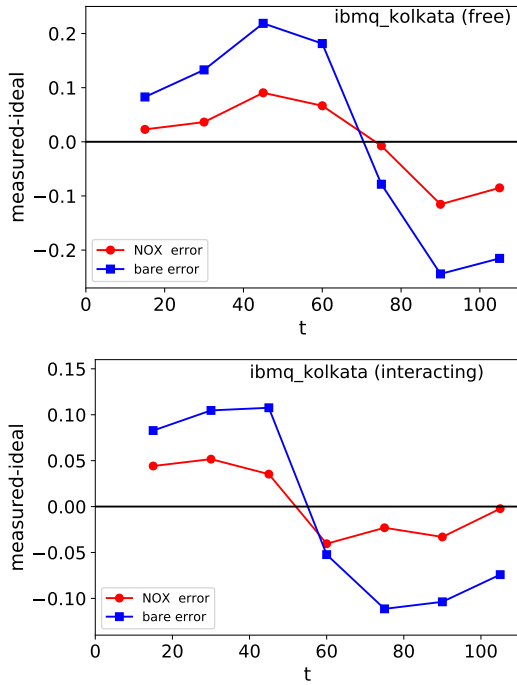


Figure 2: Bare (squares) and NOX (circle) error on  $R_-(t)$  for `ibmq_kolkata` in the free (top) and interacting (bottom) cases .

of the differences are similar for the two methods (positive for  $t \leq 60$  and negative later). However, the magnitude of these difference are significantly

smaller for the NOX procedure. Visually, it is clear that the NOX errors are about twice smaller than the bare errors.

In order to quantify this observation for the entire figure, we introduce two metrics to define the closeness of the results compared to the expected results:

$$M_1(\{Q_i\}) = \frac{1}{7} \sum_{j=1}^7 |Q_j - I_j| \quad (6)$$

and

$$M_2(\{Q_j\}) = \sqrt{\frac{1}{7} \sum_{j=1}^7 (Q_j - I_j)^2}, \quad (7)$$

where  $Q_j$  represents the NOX or bare results and  $I_j$  is the ideal value. The values for the metric are shown in Table. I. We find that the NOX data is consistently closer to the ideal results than the bare data. As seen in table I, for `ibmq_kolkata`, the error reduction – depending on the metric ( $M_1$  vs  $M_2$ ) and on the case (free vs interacting) – varied between 60% and 74%.

These computations were then repeated on two additional IBM quantum hardware platforms (`ibmq_guadalupe` and `ibmq_manila`). For `ibmq_guadalupe` we targeted qubits 7, 10, 12, 15 on the 16-qubit and for the `ibmq_manila` platform we used qubits labeled 0, 1, 2, 3 on the 5. The metrics from Eq 6 and Eq. 7 for all computers are shown in table I. Compared to the values calculated for `ibmq_kolkata`, the NOX errors on `ibmq_guadalupe` and `ibmq_manila` showed a less significant improvement.

In order to estimate the time delay due to the interaction, it is very useful to have estimated systematic errors. These are shown in Fig. 3. This allows to determine the free parameters using  $\chi^2$  minimization.

By design, the NOX mitigation technique produces more accurate expectation values for the observables under consideration. These are the  $|0100\rangle\langle 0100|$  and  $|1000\rangle\langle 1000|$  states which correspond to  $\pm k$  momentum states after the Fourier transform. Like other mitigation techniques, NOX trades precision for accuracy but then compensates for the loss in precision by increasing the number of circuits and shots. Nonetheless, getting an error bar that adequately represents the precision of the mitigated expectation values remains a challenge because the assumptions underlying NOX (as well as other mitigation techniques) aren’t guaranteed to apply perfectly, which may result in systematic loss of accuracy.

To account for these effective systematic errors, we provide NOX error bars by adding a systematic

Table I: Metrics for free and interacting case on `ibmq_kolkata`, `ibmq_guadalupe`, and `ibmq_manila`.

	<code>ibmq_kolkata</code>			<code>ibmq_guadalupe</code>			<code>ibmq_manila</code>		
Metric	NOX	Bare	NOX / Bare	NOX	Bare	NOX / Bare	NOX	Bare	NOX / Bare
$M_1$ (free)	0.061	0.165	0.368	0.102	0.191	0.533	0.206	0.274	0.749
$M_2$ (free)	0.071	0.176	0.402	0.114	0.202	0.567	0.23	0.293	0.785
$M_1$ (interacting)	0.033	0.091	0.361	0.053	0.134	0.400	0.113	0.203	0.556
$M_2$ (interacting)	0.036	0.093	0.388	0.058	0.138	0.422	0.124	0.214	0.578

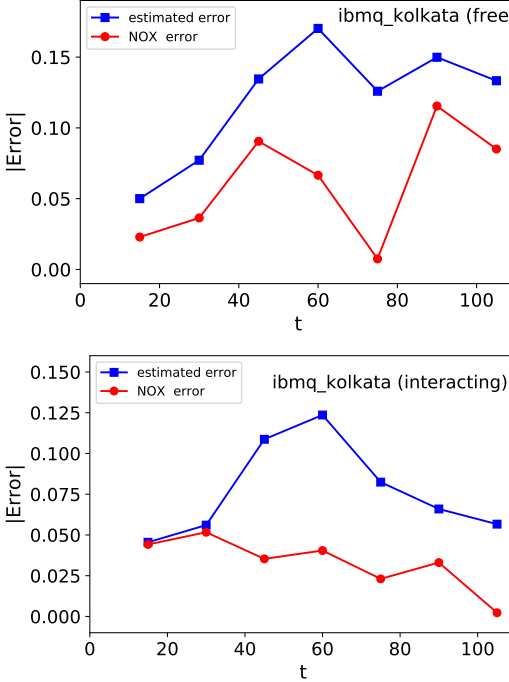


Figure 3: Actual (circles) and estimated (squares) NOX error on  $R_-(t)$  in absolute value for `ibmq_kolkata` in the free (top) and interacting (bottom) cases.

buffer to the statistical error bar obtained by taking the magnitude of the NOX correction (Eq 8).

$$\Delta_{\text{buffer}}^{\text{bias}} := \left| \hat{O}_{\text{RC+NOX}} - \hat{O}_{\text{RC}} \right| \quad (8)$$

We expand on the reasoning behind this heuristic in appendix D. We point out that for the systems under scope, this buffer value is generous, and purposefully overestimates systematic errors (see fig. 3). We comment on the discrepancies between estimated and actual error at various times in appendix E. Accurately tightening the systematic error bars of mitigated outcomes for computations vulnerable to non-Markovian or time-dependent noise sources remains an open problem.

Following [83] we assume the phase shift follows

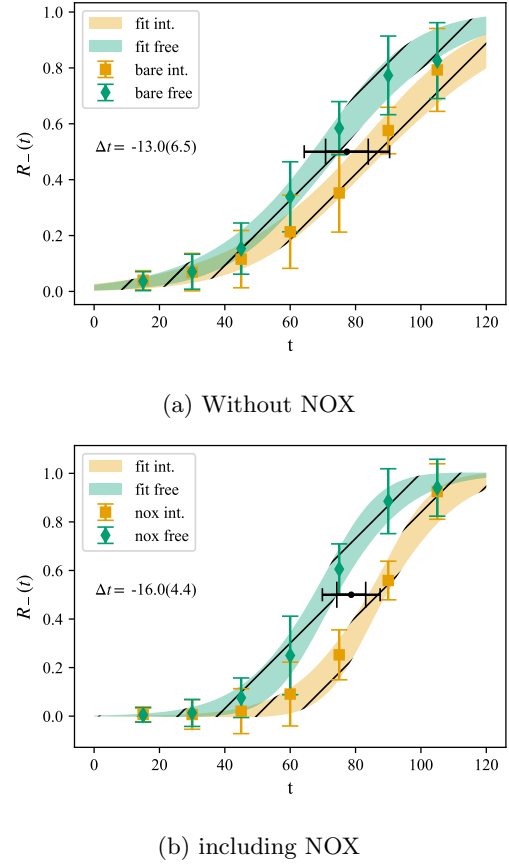


Figure 4: The time evolution and sigmoid fits for the simulation on `ibmq_kolkata` without NOX error mitigation (top) and with NOX error mitigation (bottom).

an empirical sigmoid function:

$$R_-(t) = A/(e^{-(t-\tilde{t}^*)/w} + 1). \quad (9)$$

The differences of  $\tilde{t}^*$  give us the time delay between the free and interacting wave packets. We define this difference as  $\Delta t$ .

We show the time evolution for the simulations in Fig. 4. While both results agree with the expected value of  $\Delta t = 14.8(1)$  the NOX calculation shrinks

the error bands and provides a more precise result. It is worth commenting that the accuracy of the  $\Delta t_{\text{NOX}}$  compared to  $\Delta t_{\text{BARE}}$  has improved by 33% and that the error bar has decreased by 32%. The 33% improvement in the  $\Delta t$  accuracy is more moderate than the 60% to 74% error reductions observed in the metrics  $M_1$  and  $M_2$  (see table I). This is likely an artifact that the scattering process is elastic and far from any resonances. These two factors together likely render the scattering process semi-robust to noise given that the particle does not slosh back and forth within the potential well. In this sense, the time delay  $\Delta t$  is a good example of a physical quantity that is robust against computation errors, and consequently also weakly sensitive to error mitigation.

We improved the previous real-time scattering calculations by applying three compounding error suppression techniques, namely, RCAL, RC and NOX. These improvements are applicable and can be implemented across a spectrum of STEM application domains. For a wide range of circuit depths and on three different devices, we consistently observed noticeable error reductions from NOX alone *on top* of the error reduction provided by RC and RCAL. However, the sensitivity to improved error mitigation results will likely be observable dependent. This improved accuracy for our proof-of-concept application circuits demonstrated the applicability of NOX on cloud platforms, in the advent where circuits are executed in substantially time-separated batches. We further supplemented our mitigated results with systematic error bars that accounted for unmitigated errors. Future work is planned for further refinement of systematic errors.

## ACKNOWLEDGMENTS

Y. Meurice is supported in part by the U.S. Department of Energy (DoE) under Award Number DE-SC0019139. Erik Gustafson is supported by the DOE QuantISED program through the theory consortium “Intersections of QIS and Theoretical Particle Physics” at Fermilab and by the U.S. Department of Energy. Fermilab is operated by Fermi Research Alliance, LLC under contract number DE-AC02-07CH11359 with the United States Department of Energy. P. Dreher was supported in part by the U.S. Department of Energy (DoE) under award DE-AC05-00OR22725. This material is based upon work supported by the National Science Foundation Graduate Research Fellowship under Grant No. DGE-2137100. We thank North Carolina State University (NCSU) for access to the IBM Quantum Network quantum computing hardware plat-

forms through the NCSU IBM Quantum Hub. We acknowledge the use of IBM Quantum services for this work. The views expressed are those of the authors, and do not reflect the official policy or position of IBM or the IBM Quantum team. We thank North Carolina State University (NCSU) for access to the IBM Quantum Network quantum computing hardware platforms through the NCSU IBM Quantum Hub. Y.M and E.G. thank the members of QuLAT for suggestions and comments. The project team acknowledges the use of True-Q software from Keysight Technologies [96].

## I. COMPETING INTERESTS

A. C-D. has a financial interest in Keysight Technology Inc. and the use of True-Q software [96]. The remaining authors declare no competing interests.

## II. DATA AVAILABILITY

Data is available from the corresponding author upon reasonable request.

## Supplementary Material

### Appendix A: Physics Background

The QIM in one spatial dimension shown in Eq. A1,

$$\hat{H}_0 = -J \sum_{i=1}^{N-1} \hat{\sigma}_i^x \hat{\sigma}_{i+1}^x - h_T \sum_{i=1}^N \hat{\sigma}_i^z. \quad (\text{A1})$$

is very well understood [101] and implemented on NISQ devices. [8–11]. Because this model is constructed invariant under translations, the standard quantum mechanics two-particle-scattering problem can be reduced to a single particle Schrödinger equation in an effective potential. In one spatial dimension, the simplest case of effective potential that can generate a phase shift for the reduced problem is a potential step adjacent to an infinite wall. This can be written as an interaction term:

$$\hat{H}_{int} = U \left( \frac{1 - \hat{\sigma}_{N_S}^z}{2} \right) \quad (\text{A2})$$

When constructing the initial wave packet it is necessary to have some localization in space so that a distinct scattering event is visible. Because of this

construct the wave packet will have some momentum distribution because it no longer is a plane wave. A quantum Fourier transform (QFTr) is performed to transform this state into momentum space. We define the probabilities to be in the  $|\pm k\rangle$  state

$$P_{\pm}(t) \equiv |\langle \pm k | \psi(t) \rangle|^2, \quad (\text{A3})$$

and their normalized versions

$$R_{\pm}(t) \equiv \frac{P_{\pm}(t)}{P_+(t) + P_-(t)} \quad (\text{A4})$$

which by design satisfy

$$R_+ + R_- = 1. \quad (\text{A5})$$

The real-time evolution provides the time  $t^*$  necessary to reach the symmetric situation where  $P_+(t^*) = P_-(t^*)$  and  $R_-(t^*) = 0.5$ . It is noted that the time  $t^*$  is determined by the symmetric condition  $R_-(t^*) = R_+(t^*) = 0.5$ . This also corresponds to the time where a classical particle would hit the wall. We can then compare  $t^*$  in the case where  $U = 0$  and a non-zero value. We call these times  $t_{free}^*$  and  $t_{int.}^*$ , respectively. With this normalization from Eq. A5 the  $R_+(t)$  and  $R_-(t)$  get interchanged under time-reversal with respect to  $t^*$ . We define the difference

$$\Delta t^* \equiv t_{int.}^* - t_{free}^*, \quad (\text{A6})$$

and will argue that

$$\Delta t^* = \frac{\Delta t_W}{2} \quad (\text{A7})$$

where  $\Delta t_W$  is the Wigner time delay [102] [103]

Because of the small volume, we used a *deformed* sigmoid parametrization for  $R_-(t)$  in Eq. A8

$$R_-(t) \simeq A/(1 + \exp(-(\frac{t - \tilde{t}^*}{w}))) \quad (\text{A8})$$

It is noted that the number of two-qubit gates in these Fourier transforms will expand quickly as a function of the number of qubits in the scattering problem, the most challenging part of the computation was to mitigate the noise in these Fourier transform circuits to quantitatively measure the systematic errors. We provide the gate decompositions for the *F*-gate and the *CZ* gate and show the implementation of the *F*-gate on the IBM quantum hardware in Fig. 5.

In addition, errors induced by imperfect Trotter steps were also challenging. These systematic errors are expected to dominate the error profile of the scattering phase shift compared to the statistical errors and the focus of this project will be to utilize methodologies that can quantitatively estimate these systematic errors.

## Appendix B: Quantum gates, cycles and circuits

The circuit model of quantum computation consists of expressing a program as an ordered list of instructions. A *circuit* refers to such an ordered list. Each instruction consists of a tuple containing the registers to address (e.g. the qubit indices) and the operation to perform. Possible operations include *gates* (which are unitary operations on the register space), measurement, and state preparation (e.g. qubit reset). Finally, a computing *cycle* (also known as clock cycle) usually refers to parallel instructions, although it can also refer to a set of sequential instructions addressing disjoint sets of registers.

Error processes depend on the gates but can affect different registers than the instruction is meant to address. The errors also depend on the precise relative scheduling of the instructions during a cycle. Fortunately, it is generally observed that error channels only weakly depend on prior cycles. For this reason, we attach fixed error channels to cycles rather than to gates. That is, we express the error-prone version of the ideal cycle  $C_i$  as  $\mathcal{E}_i C_i$ . The  $\mathcal{E}_i$  depends on the cycle  $C_i$ .

As we will see in the next appendix, NOX combines different circuits  $C_i$  where the  $i$ th cycle  $C_i$  has an amplified error  $\mathcal{E}_i^{1+\alpha}$ .

## Appendix C: First-order correction through NOX

In this section, we provide a brief analysis of NOX, and show what kind of correction it provides on the bare circuit. First, let's re-express the effective RC circuit as

$$\langle \mathcal{C} \rangle_{\text{RC}} = \mathcal{C}_{\text{ideal}} + \sum_{i=1}^m \Delta_i + \sum_{i>j} \sum_{j=1}^m \Delta_i \Delta_j + h.o. \quad (\text{C1})$$

where

$$\Delta_i := C_m \cdots C_{i+1} (\mathcal{E}_i - 1) C_i \cdots C_1. \quad (\text{C2})$$

The next higher-order term in the expansion of eq. (C1) scale as  $(\frac{m}{3}) \Delta^3$ . If the assumptions underlying NOX are perfectly respected, then we obtain amplified circuits of the form

$$\begin{aligned} \langle \mathcal{C}_i \rangle_{\text{RC}} = & \mathcal{C}_{\text{ideal}} + \alpha \Delta_i + \sum_{j=1}^m \Delta_j + \alpha \sum_{j>i}^m \Delta_j \Delta_i \\ & + \alpha \sum_{i>j}^m \Delta_i \Delta_j + \sum_{k>j}^m \sum_{j=1}^m \Delta_k \Delta_j + h.o., \end{aligned} \quad (\text{C3})$$

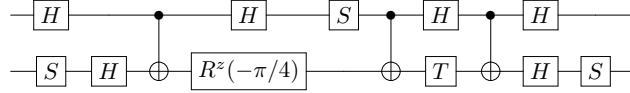


Figure 5: Decomposition of F-gate for IBM quantum computer.

where the higher-order terms include a  $O(m^3\Delta^3)$  scaling, but also a  $O(m\Delta^2)$  scaling from the Taylor expansion of  $\mathcal{E}_i^{1+\alpha}$ . If we substitute eqs. (C1) and (C3) in eq. (4), we immediately get:

$$\begin{aligned} \langle \mathcal{C} \rangle_{\text{NOX}} &:= \frac{\alpha + m}{\alpha} \langle \mathcal{C} \rangle_{\text{RC}} - \frac{1}{\alpha} \sum_{i=1}^m \langle \mathcal{C}_i \rangle_{\text{RC}} \\ &= \mathcal{C}_{\text{ideal}} - \sum_{i>j} \sum_{j=1}^m \Delta_i \Delta_j + h.o. \quad (\text{C4}) \end{aligned}$$

which indicates a remaining bias that scales as  $O(m^2\Delta^2)$ , as opposed to  $O(m\Delta)$  in the unmitigated case.

#### Appendix D: Error Estimation Using Noiseless Output Extrapolation

As shown in the previous section, NOX ideally induces a first-order correction on the output. However, this mitigation effect is founded around a Markovian time-independent error model, as well as on a perfect error amplification  $\mathcal{E}_i \rightarrow \mathcal{E}_i^{1+\alpha}$  through cycle repetition. A number of physical mechanisms can bring us outside of this framework, and reduce the accuracy of NOX-mitigated results.

For instance, one mechanism in which accuracy can be lost is if an error channel  $\mathcal{E}_i$  doesn't exactly commute with the cycle  $C_i$ . In this case, the amplified error resulting from repeating  $\mathcal{E}_i^{\text{amp}} = C_i^{-(1+\alpha)} (\mathcal{E}_i C_i)^{1+\alpha}$ , might slightly differ from the amplified channel  $\mathcal{E}_i^{1+\alpha}$ . Other mechanisms for systematic loss in accuracy include time-dependent effects such as error drift and re-calibration, as well as non-Markovian effects.

To account for effective systematic errors, we provide NOX error bars by adding a systematic buffer to the statistical error bar obtained by taking the magnitude of the NOX correction:

$$\Delta_{\text{buffer}}^{\text{bias}} := |\hat{O}_{\text{RC+NOX}} - \hat{O}_{\text{RC}}| . \quad (\text{D1})$$

To see the reasoning behind this choice of buffer value, recall eq. (C3). To accommodate for faulty error amplification mechanisms, we modify eq. (C3)

by adding new terms:

$$\langle \mathcal{C}_i \rangle_{\text{RC}} = \mathcal{C}_{\text{ideal}} + \alpha \Delta_i + \alpha \Delta_i^{(1)} + \Delta_i^{(2)} + \sum_{j=1}^m \Delta_j + h.o. \quad (\text{D2})$$

Here the term  $\alpha \Delta_i^{(1)}$  would represent the effect of a systematic fluctuation in the amplification mechanism; the  $\Delta_i^{(2)}$  term would instead correspond to systematic fluctuations in non-amplified error components due to e.g time-dependent effects arising between circuits. By substituting eq. (D2) in eq. (4), we obtain

$$\hat{O}_{\text{RC+NOX}} = \hat{O}_{\text{ideal}} - \sum_i \mathbb{E} \left( O \left| \Delta_i^{(1)} + \frac{\Delta_i^{(2)}}{\alpha} \right. \right) + h.o. \quad (\text{D3})$$

where the higher order terms are of second order in the circuit error probability. Let's define the following error ratio

$$\Gamma := \frac{|\sum_i \mathbb{E}(O|\Delta_i)|}{\left| \sum_i \mathbb{E} \left( O \left| \Delta_i^{(1)} + \frac{\Delta_i^{(2)}}{\alpha} \right. \right) \right|} . \quad (\text{D4})$$

The numerator is the first-order error term meant to be removed by NOX. The denominator is zero in the absence of violations to the framework that led to eq. (C3). With the expectation of weak violations – weaker than the “baseline” noise induced by  $\Delta_i$  – we certainly expect  $\Gamma$  to be greater than 1, but by how much? Here, we consider the eventuality that the effect of leftover error  $\sum_i \Delta_i^{(1)} + \frac{\Delta_i^{(2)}}{\alpha}$  on the observable  $O$  is at least comparable to the effect of the first order bare error  $\sum_i \Delta_i$ . That is, instead of assuming  $\Gamma \gg 1$  – which holds when there are close to no violations of the assumptions that led to eq. (C3) – we make the much more cautious assumption  $\Gamma \geq 2$ . In other words, we assume that effects such as imperfect averaging due to time-dependent error rate fluctuations aren't necessarily negligible, but are at least twice smaller than baseline error rates. From there, we get our first-order upper bound on the sys-

tematic error in NOX:

$$\begin{aligned}
& |\hat{O}_{\text{RC+NOX}} - \hat{O}_{\text{RC}}| \simeq \left| \sum_i \mathbb{E} \left( O \left| \Delta_i - \Delta_i^{(1)} - \frac{\Delta_i^{(2)}}{\alpha} \right. \right) \right| \\
& \quad (\text{eq. (4), eq. (C1), eq. (D2)}) \\
& \geq \left| \sum_i \mathbb{E}(O|\Delta_i) \right| - \left| \sum_i \mathbb{E} \left( O \left| \Delta_i^{(1)} + \frac{\Delta_i^{(2)}}{\alpha} \right. \right) \right| \\
& \quad (\text{rev. triang. ineq.}) \\
& = |\Gamma - 1| \left| \sum_i \mathbb{E} \left( O \left| \Delta_i^{(1)} + \frac{\Delta_i^{(2)}}{\alpha} \right. \right) \right| \\
& \quad (\text{def. of } \Gamma, \text{ eq. (D4)}) \\
& \geq \left| \sum_i \mathbb{E} \left( O \left| \Delta_i^{(1)} + \frac{\Delta_i^{(2)}}{\alpha} \right. \right) \right|. \\
& \quad (\text{Assumption } \Gamma \geq 2)
\end{aligned}$$

Note that the assumption  $\Gamma \geq 2$  is coarse and inspired by empirical data (see fig. 3). Refining device-specific or application-specific upper bounds on  $\Gamma$  is left as an open research avenue.

#### Appendix E: Remarks about the time-dependent features of the errors.

In this section, we provide results from ideal numerical calculations for  $1/(P_+ + P_-)$  in the free and interacting cases. We noticed empirically that large values of  $1/(P_+ + P_-)$  appear to be correlated with significant overestimations of the NOX errors. The peaks of  $1/(P_+ + P_-)$ , the change of sign in the errors and the largest error overestimations appear near the values of  $t^*$  which are approximately 69 and 55 in the free and interacting cases respectively [83].

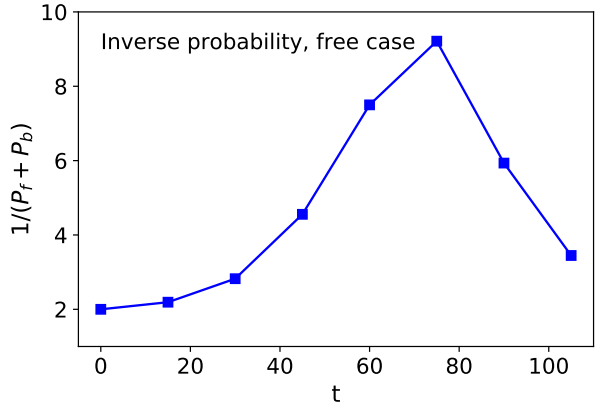


Figure 6:  $1/(P_+ + P_-)$  in the free case.

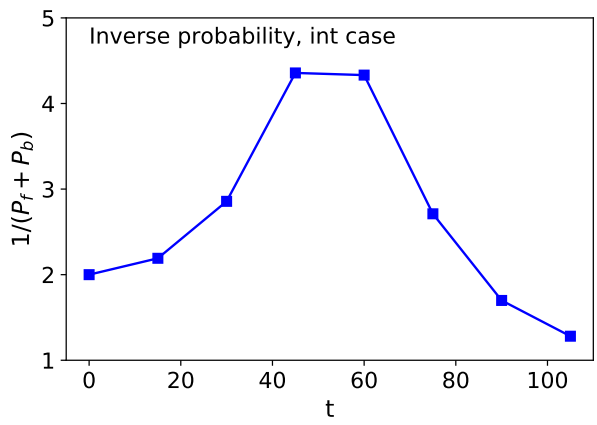


Figure 7:  $1/(P_+ + P_-)$  in the interacting case.

- 
- [1] M. S. Alam, S. Belomestnykh, N. Bornman, G. Cancelo, Y.-C. Chao, M. Checchin, V. S. Dinh, A. Grassellino, E. J. Gustafson, R. Harnik, C. R. H. McRae, Z. Huang, K. Kapoor, T. Kim, J. B. Kowalkowski, M. J. Kramer, Y. Krasnikova, P. Kumar, D. M. Kurkcuoglu, H. Lamm, A. L. Lyon, D. Milathianaki, A. Murthy, J. Mutus, I. Nekrashevich, J. Oh, A. B. Özgüler, G. N. Perdue, M. Reagor, A. Romanenko, J. A. Sauls, L. Stefanazzi, N. M. Tubman, D. Venturelli, C. Wang, X. You, D. M. T. van Zanten, L. Zhou, S. Zhu, and S. Zorzetti, “Quantum computing hardware for hep algorithms and sensing,” (2022).
- [2] C. W. Bauer, Z. Davoudi, A. B. Balantekin, T. Bhattacharya, M. Carena, W. A. de Jong, P. Draper, A. El-Khadra, N. Gemelke, M. Hanada,
- D. Kharzeev, H. Lamm, Y.-Y. Li, J. Liu, M. Lukin, Y. Meurice, C. Monroe, B. Nachman, G. Pagano, J. Preskill, E. Rinaldi, A. Roggero, D. I. Santiago, M. J. Savage, I. Siddiqi, G. Siopsis, D. Van Zanten, N. Wiebe, Y. Yamauchi, K. Yeter-Aydeniz, and S. Zorzetti, “Quantum simulation for high energy physics,” (2022).
- [3] T. S. Humble, A. Delgado, R. Pooser, C. Seck, R. Bennink, V. Leyton-Ortega, C. C. J. Wang, E. Dumitrescu, T. Morris, K. Hamilton, D. Lyakh, P. Date, Y. Wang, N. A. Peters, K. J. Evans, M. Demarteau, A. McCaskey, T. Nguyen, S. Clark, M. Reville, A. Di Meglio, M. Grossi, S. Vallecorsa, K. Borras, K. Jansen, and D. Krücker, “Snowmass white paper: Quantum computing systems and software for high-energy physics research,”

- (2022).
- [4] N. Klco, A. Roggero, and M. J. Savage, *Rept. Prog. Phys.* **85**, 064301 (2022), arXiv:2107.04769 [quant-ph].
  - [5] M. C. Bañuls and K. Cichy, *Rept. Prog. Phys.* **83**, 024401 (2020), arXiv:1910.00257 [hep-lat].
  - [6] M. C. Bañuls *et al.*, *Eur. Phys. J. D* **74**, 165 (2020), arXiv:1911.00003 [quant-ph].
  - [7] I. M. Georgescu, S. Ashhab, and F. Nori, *Rev. Mod. Phys.* **86**, 153 (2014).
  - [8] A. Cervera-Lierta, *Quantum* **2**, 114 (2018).
  - [9] H. Lamm and S. Lawrence, *Phys. Rev. Lett.* **121**, 170501 (2018), arXiv:1806.06649 [quant-ph].
  - [10] E. Gustafson, Y. Meurice, and J. Unmuth-Yockey, *Physical Review D* **99** (2019), 10.1103/PhysRevD.99.094503.
  - [11] E. Gustafson, P. Dreher, Z. Hang, and Y. Meurice, “Benchmarking quantum computers for real-time evolution of a  $(1+1)$  field theory with error mitigation,” (2019), arXiv:1910.09478 [hep-lat].
  - [12] M. Kim, Y. Song, J. Kim, and J. Ahn, *PRX Quantum* **1** (2020), 10.1103/prxquantum.1.020323.
  - [13] K. Yeter-Aydeniz, G. Siopsis, and R. C. Pooser, “Scattering in the Ising model using quantum Lanczos algorithm,” (2021), arXiv:2008.08763 [quant-ph].
  - [14] J. Vovrosh and J. Knolle, (2020), arXiv:2001.03044 [cond-mat.str-el].
  - [15] Y. Salathé, M. Mondal, M. Oppiger, J. Heinsoo, P. Kurpiers, A. Potočnik, A. Mezzacapo, U. Las Heras, L. Lamata, E. Solano, and et al., *Physical Review X* **5** (2015), 10.1103/physrevx.5.021027.
  - [16] W. L. Tan, P. Becker, F. Liu, G. Pagano, K. S. Collins, A. De, L. Feng, H. B. Kaplan, A. Kyprianidis, R. Lundgren, and et al., *Nature Physics* (2021), 10.1038/s41567-021-01194-3.
  - [17] A. Smith, M. S. Kim, F. Pollmann, and J. Knolle, *npj Quantum Information* **5** (2019), 10.1038/s41534-019-0217-0.
  - [18] H. Labuhn, D. Barredo, S. Ravets, S. de Léséleuc, T. Macrì, T. Lahaye, and A. Browaeys, *Nature* **534**, 667–670 (2016).
  - [19] J. Zhang, G. Pagano, P. W. Hess, A. Kyprianidis, P. Becker, H. Kaplan, A. V. Gorshkov, Z. X. Gong, and C. Monroe, *Nature (London)* **551**, 601 (2017), arXiv:1708.01044 [quant-ph].
  - [20] T. Kadowaki and H. Nishimori, *Phys. Rev. E* **58**, 5355 (1998).
  - [21] H. Bernien, S. Schwartz, A. Keesling, H. Levine, A. Omran, H. Pichler, S. Choi, A. S. Zibrov, M. Endres, M. Greiner, V. Vuletić, and M. D. Lukin, *Nature (London)* **551**, 579 (2017), arXiv:1707.04344 [quant-ph].
  - [22] A. N. Ciavarella, S. Caspar, H. Singh, M. J. Savage, and P. Lougovski, (2022), arXiv:2207.09438 [quant-ph].
  - [23] A. Alexandru, P. F. Bedaque, S. Harmalkar, H. Lamm, S. Lawrence, and N. C. Warrington, *Physical Review D* **100** (2019), 10.1103/physrevd.100.114501.
  - [24] E. Zohar, J. I. Cirac, and B. Reznik, *Physical Review A* **88** (2013), 10.1103/physreva.88.023617.
  - [25] E. A. Martinez, C. A. Muschik, P. Schindler, D. Nigg, A. Erhard, M. Heyl, P. Hauke, M. Dalmonte, T. Monz, P. Zoller, and R. Blatt, *Nature* **534**, 516 EP (2016).
  - [26] B. Buyens, J. Haegeman, F. Verstraete, and K. Van Acoleyen, *Phys. Rev. D* **96**, 114501 (2017), arXiv:1612.00739 [hep-lat].
  - [27] A. Jahin, A. C. Y. Li, T. Iadecola, P. P. Orth, G. N. Perdue, A. Macridin, M. S. Alam, and N. M. Tubman, *Physical Review A* **106** (2022), 10.1103/physreva.106.022434.
  - [28] N. Klco, E. F. Dumitrescu, A. J. McCaskey, T. D. Morris, R. C. Pooser, M. Sanz, E. Solano, P. Lougovski, and M. J. Savage, *Phys. Rev. A* **98**, 032331 (2018), arXiv:1803.03326 [quant-ph].
  - [29] R. C. Brower, D. Berenstein, and H. Kawai, PoS **LATTICE2019**, 112 (2019), arXiv:2002.10028 [hep-lat].
  - [30] P. I. Karpov, G. Y. Zhu, M. P. Heller, and M. Heyl, (2020), arXiv:2011.11624 [cond-mat.quant-gas].
  - [31] E. T. Holland, K. A. Wendt, K. Kravvaris, X. Wu, W. E. Ormand, J. L. DuBois, S. Quaglioni, and F. Pederiva, *Physical Review A* **101** (2020), 10.1103/physreva.101.062307.
  - [32] A. Roggero, C. Gu, A. Baroni, and T. Papenbrock, *Physical Review C* **102** (2020), 10.1103/physrevc.102.064624.
  - [33] F. M. Surace and A. Lerose, (2021), arXiv:2011.10583 [cond-mat.quant-gas].
  - [34] D. E. Kharzeev and Y. Kikuchi, *Phys. Rev. Res.* **2**, 023342 (2020), arXiv:2001.00698 [hep-ph].
  - [35] K. Ikeda, D. E. Kharzeev, and Y. Kikuchi, (2020), arXiv:2012.02926 [hep-ph].
  - [36] R. A. Briceño, J. V. Guerrero, M. T. Hansen, and A. M. Sturzu, *Phys. Rev. D* **103**, 014506 (2021), arXiv:2007.01155 [hep-lat].
  - [37] M. Van Damme, L. Vanderstraeten, J. De Nardis, J. Haegeman, and F. Verstraete, *Phys. Rev. Research* **3**, 013078 (2021).
  - [38] E. Zohar, J. I. Cirac, and B. Reznik, *Phys. Rev. Lett.* **109**, 125302 (2012), arXiv:1204.6574 [quant-ph].
  - [39] E. Zohar, J. I. Cirac, and B. Reznik, *Phys. Rev. Lett.* **110**, 125304 (2013), arXiv:1211.2241 [quant-ph].
  - [40] E. Zohar, J. I. Cirac, and B. Reznik, *Phys. Rev. A* **88**, 023617 (2013), arXiv:1303.5040 [quant-ph].
  - [41] E. Zohar and M. Burrello, *Phys. Rev. D* **91**, 054506 (2015), arXiv:1409.3085 [quant-ph].
  - [42] E. Zohar, J. I. Cirac, and B. Reznik, *Rept. Prog. Phys.* **79**, 014401 (2016), arXiv:1503.02312 [quant-ph].
  - [43] E. Zohar, A. Farace, B. Reznik, and J. I. Cirac, *Phys. Rev. A* **95**, 023604 (2017), arXiv:1607.08121 [quant-ph].
  - [44] N. Klco, J. R. Stryker, and M. J. Savage, *Phys. Rev. D* **101**, 074512 (2020), arXiv:1908.06935 [quant-ph].

- [45] A. Ciavarella, N. Klco, and M. J. Savage, “A Trail-head for Quantum Simulation of SU(3) Yang-Mills Lattice Gauge Theory in the Local Multiplet Basis,” (2021), [arXiv:2101.10227 \[quant-ph\]](#).
- [46] J. Bender, E. Zohar, A. Farace, and J. I. Cirac, *New J. Phys.* **20**, 093001 (2018), [arXiv:1804.02082 \[quant-ph\]](#).
- [47] J. Liu and Y. Xin, “Quantum simulation of quantum field theories as quantum chemistry,” (2020), [arXiv:2004.13234 \[hep-th\]](#).
- [48] D. C. Hackett, K. Howe, C. Hughes, W. Jay, E. T. Neil, and J. N. Simone, *Phys. Rev. A* **99**, 062341 (2019), [arXiv:1811.03629 \[quant-ph\]](#).
- [49] A. Alexandru, P. F. Bedaque, S. Harmalkar, H. Lamm, S. Lawrence, and N. C. Warrington (NuQS), *Phys. Rev. D* **100**, 114501 (2019), [arXiv:1906.11213 \[hep-lat\]](#).
- [50] A. Yamamoto, *PTEP* **2021**, 013B06 (2021), [arXiv:2008.11395 \[hep-lat\]](#).
- [51] J. F. Haase, L. Dellantonio, A. Celi, D. Paulson, A. Kan, K. Jansen, and C. A. Muschik, *Quantum* **5**, 393 (2021), [arXiv:2006.14160 \[quant-ph\]](#).
- [52] T. Armon, S. Ashkenazi, G. García-Moreno, A. González-Tudela, and E. Zohar, “Photon-mediated Stroboscopic Quantum Simulation of a  $\mathbb{Z}_2$  Lattice Gauge Theory,” (2021), [arXiv:2107.13024 \[quant-ph\]](#).
- [53] A. Bazavov, S. Catterall, R. G. Jha, and J. Unmuth-Yockey, *Phys. Rev. D* **99**, 114507 (2019).
- [54] A. Bazavov, Y. Meurice, S.-W. Tsai, J. Unmuth-Yockey, and J. Zhang, *Phys. Rev. D* **92**, 076003 (2015), [arXiv:1503.08354 \[hep-lat\]](#).
- [55] J. Zhang, J. Unmuth-Yockey, J. Zeiher, A. Bazavov, S. W. Tsai, and Y. Meurice, *Phys. Rev. Lett.* **121**, 223201 (2018), [arXiv:1803.11166 \[hep-lat\]](#).
- [56] J. Unmuth-Yockey, J. Zhang, A. Bazavov, Y. Meurice, and S.-W. Tsai, *Phys. Rev. D* **98**, 094511 (2018), [arXiv:1807.09186 \[hep-lat\]](#).
- [57] J. F. Unmuth-Yockey, *Phys. Rev. D* **99**, 074502 (2019), [arXiv:1811.05884 \[hep-lat\]](#).
- [58] M. Kreshchuk, W. M. Kirby, G. Goldstein, H. Beauchemin, and P. J. Love, “Quantum Simulation of Quantum Field Theory in the Light-Front Formulation,” (2020), [arXiv:2002.04016 \[quant-ph\]](#).
- [59] M. Kreshchuk, S. Jia, W. M. Kirby, G. Goldstein, J. P. Vary, and P. J. Love, “Simulating Hadronic Physics on NISQ devices using Basis Light-Front Quantization,” (2020), [arXiv:2011.13443 \[quant-ph\]](#).
- [60] I. Raychowdhury and J. R. Stryker, “Solving Gauss’s Law on Digital Quantum Computers with Loop-String-Hadron Digitization,” (2018), [arXiv:1812.07554 \[hep-lat\]](#).
- [61] I. Raychowdhury and J. R. Stryker, *Phys. Rev. D* **101**, 114502 (2020), [arXiv:1912.06133 \[hep-lat\]](#).
- [62] Z. Davoudi, I. Raychowdhury, and A. Shaw, “Search for Efficient Formulations for Hamiltonian Simulation of non-Abelian Lattice Gauge Theories,” (2020), [arXiv:2009.11802 \[hep-lat\]](#).
- [63] U.-J. Wiese, *Proceedings, 24th International Conference on Ultra-Relativistic Nucleus-Nucleus Collisions (Quark Matter 2014): Darmstadt, Germany, May 19-24, 2014*, *Nucl. Phys.* **A931**, 246 (2014), [arXiv:1409.7414 \[hep-th\]](#).
- [64] D. Luo, J. Shen, M. Highman, B. K. Clark, B. DeMarco, A. X. El-Khadra, and B. Gadway, “A Framework for Simulating Gauge Theories with Dipolar Spin Systems,” (2019), [arXiv:1912.11488 \[quant-ph\]](#).
- [65] S. V. Mathis, G. Mazzola, and I. Tavernelli, *Phys. Rev. D* **102**, 094501 (2020), [arXiv:2005.10271 \[quant-ph\]](#).
- [66] H. Singh, “Qubit  $O(N)$  nonlinear sigma models,” (2019), [arXiv:1911.12353 \[hep-lat\]](#).
- [67] H. Singh and S. Chandrasekharan, *Phys. Rev. D* **100**, 054505 (2019), [arXiv:1905.13204 \[hep-lat\]](#).
- [68] A. J. Buser, T. Bhattacharya, L. Cincio, and R. Gupta, “Quantum simulation of the qubit-regularized  $O(3)$ -sigma model,” (2020), [arXiv:2006.15746 \[quant-ph\]](#).
- [69] T. Bhattacharya, A. J. Buser, S. Chandrasekharan, R. Gupta, and H. Singh, “Qubit regularization of asymptotic freedom,” (2020), [arXiv:2012.02153 \[hep-lat\]](#).
- [70] J. a. Barata, N. Mueller, A. Tarasov, and R. Venugopalan, “Single-particle digitization strategy for quantum computation of a  $\phi^4$  scalar field theory,” (2020), [arXiv:2012.00020 \[hep-th\]](#).
- [71] M. Kreshchuk, S. Jia, W. M. Kirby, G. Goldstein, J. P. Vary, and P. J. Love, “Light-Front Field Theory on Current Quantum Computers,” (2020), [arXiv:2009.07885 \[quant-ph\]](#).
- [72] Y. Ji, H. Lamm, and S. Zhu (NuQS), *Phys. Rev. D* **102**, 114513 (2020), [arXiv:2005.14221 \[hep-lat\]](#).
- [73] C. W. Bauer and D. M. Grabowska, “Efficient Representation for Simulating U(1) Gauge Theories on Digital Quantum Computers at All Values of the Coupling,” (2021), [arXiv:2111.08015 \[hep-ph\]](#).
- [74] E. Gustafson, *Phys. Rev. D* **103**, 114505 (2021), [arXiv:2104.10136 \[quant-ph\]](#).
- [75] T. Hartung, T. Jakobs, K. Jansen, J. Ostmeyer, and C. Urbach, *Eur. Phys. J. C* **82**, 237 (2022), [arXiv:2201.09625 \[hep-lat\]](#).
- [76] D. M. Grabowska, C. Kane, B. Nachman, and C. W. Bauer, “Overcoming exponential scaling with system size in Trotter-Suzuki implementations of constrained Hamiltonians: 2+1 U(1) lattice gauge theories,” (2022), [arXiv:2208.03333 \[quant-ph\]](#).
- [77] E. M. Murairi, M. J. Cervia, H. Kumar, P. F. Bedaque, and A. Alexandru, “How many quantum gates do gauge theories require?” (2022), [arXiv:2208.11789 \[hep-lat\]](#).
- [78] E. Gustafson, “Noise Improvements in Quantum Simulations of sQED using Qutrits,” (2022), [arXiv:2201.04546 \[quant-ph\]](#).
- [79] R. C. Farrell, I. A. Chernyshev, S. J. M. Powell, N. A. Zemlevskiy, M. Illa, and M. J. Savage, (2022), [arXiv:2209.10781 \[quant-ph\]](#).

- [80] E. J. Gustafson, H. Lamm, F. Lovelace, and D. Musk, (2022), arXiv:2208.12309 [quant-ph].
- [81] B. McDonough, A. Mari, N. Shammah, N. T. Stemen, M. Wahl, W. J. Zeng, and P. P. Orth, (2022), arXiv:2210.08611 [quant-ph].
- [82] I.-C. Chen, B. Burdick, Y. Yao, P. P. Orth, and T. Iadecola, *Physical Review Research* **4** (2022), 10.1103/physrevresearch.4.043027.
- [83] E. Gustafson, Y. Zhu, P. Dreher, N. M. Linke, and Y. Meurice, *Physical Review D* **104** (2021), 10.1103/physrevd.104.054507.
- [84] Y. Meurice, *Quantum field theory: a quantum computation approach* (Institute of Physics Publishing, Bristol, 2021).
- [85] Y. Meurice, R. Sakai, and J. Unmuth-Yockey, (2020), arXiv:2010.06539 [hep-lat].
- [86] S. Bravyi, S. Sheldon, A. Kandala, D. C. McKay, and J. M. Gambetta, *Phys. Rev. A* **103**, 042605 (2021).
- [87] P. D. Nation, H. Kang, N. Sundaresan, and J. M. Gambetta, *PRX Quantum* **2**, 040326 (2021), arXiv:2108.12518 [quant-ph].
- [88] B. Nachman, M. Urbanek, W. A. de Jong, and C. W. Bauer, *npj Quantum Information* **6**, 84 (2020), arXiv:1910.01969 [quant-ph].
- [89] R. Hicks, C. W. Bauer, and B. Nachman, *Phys. Rev. A* **103**, 022407 (2021).
- [90] K. Wang, Y.-A. Chen, and X. Wang, “Measurement error mitigation via truncated neumann series,” (2021).
- [91] M. R. Geller and M. Sun, *Quantum Science and Technology* **6**, 025009 (2021).
- [92] F. B. Maciejewski, Z. Zimborás, and M. Oszmaniec, *Quantum* **4**, 257 (2020).
- [93] E. van den Berg, Z. K. Minev, and K. Temme, *Physical Review A* **105** (2022), 10.1103/physreva.105.032620.
- [94] J. J. Wallman and J. Emerson, *Physical Review A* **94** (2016), 10.1103/physreva.94.052325.
- [95] S. Ferracin, A. Hashim, J.-L. Ville, R. Naik, A. Carignan-Dugas, H. Qassim, A. Morvan, D. I. Santiago, I. Siddiqi, and J. J. Wallman, “Efficiently improving the performance of noisy quantum computers,” (2022).
- [96] S. J. Beale, K. Boone, A. Carignan-Dugas, A. Chytros, D. Dahlen, H. Dawkins, J. Emerson, S. Ferracin, V. Frey, I. Hincks, D. Hufnagel, P. Iyer, A. Jain, J. Kolbush, E. Ospadov, J. L. Pino, H. Qassim, J. Saunders, J. Skanes-Norman, A. Stasiuk, J. J. Wallman, A. Winick, and E. Wright, “True-q,” <https://doi.org/10.5281/zenodo.3945250> (2020).
- [97] A. Hashim, R. K. Naik, A. Morvan, J.-L. Ville, B. Mitchell, J. M. Kreikebaum, M. Davis, E. Smith, C. Iancu, K. P. O’Brien, I. Hincks, J. J. Wallman, J. Emerson, and I. Siddiqi, *Physical Review X* **11** (2021), 10.1103/physrevx.11.041039.
- [98] J.-L. Ville, A. Morvan, A. Hashim, R. K. Naik, M. Lu, B. Mitchell, J.-M. Kreikebaum, K. P. O’Brien, J. J. Wallman, I. Hincks, J. Emerson, E. Smith, E. Younis, C. Iancu, D. I. Santiago, and I. Siddiqi, “Leveraging randomized compiling for the qite algorithm,” (2021).
- [99] Y. Gu, Y. Ma, N. Forcellini, and D. E. Liu, (2022), 10.48550/ARXIV.2208.04100.
- [100] In RC, the circuit subdivisions are called *dressed cycles*, and must take a specific form. See [94].
- [101] J. B. Kogut, *Rev. Mod. Phys.* **55**, 775 (1983).
- [102] E. P. Wigner, *Phys. Rev.* **98**, 145 (1955).
- [103] This relation can be justified from the time-reversal argument that after  $t_{int}^*$ , only *half* of the phase shift,  $\delta(k)$ , has built up while the other half builds after  $t^*$ . This is actually why historically, the total phase shift is denoted  $2\delta(k)$ .